ADVANCED HEALTHCARE MATERIALS
www.advhealthmat.de

Nucleolus-Targeted Photodynamic Anticancer Therapy Using Renal-Clearable Carbon Dots

Wen Pang, Pengfei Jiang, Shihui Ding, Zhouzhou Bao, Ningtao Wang, Hongxia Wang, Junle Qu, Dan Wang, Bobo Gu,* and Xunbin Wei**

Photodynamic therapy (PDT), which utilizes light excited photosensitizers (PSs) to generate reactive oxygen species (ROS) and consequently ablate cancer cells or diseased tissue, has attracted a great deal of attention in the last decades due to its unique advantages. In order to further enhance PDT effect, PSs are functionalized to target specific sub-cellular organelles, but most PSs cannot target nucleolus, which is demonstrated as a more efficient and ideal site for cancer treatment. Here, an effective carbon dots (C-dots) photosensitizer with intrinsic nucleolus-targeting capability, for the first time, is synthesized, characterized, and employed for in vitro and in vivo image-guided photodynamic anticancer therapy with enhanced treatment performance at a low dose of PS and light irradiation. The C-dots possess high ROS generation efficiency and fluorescence quantum yield, excellent in vitro and in vivo biocompatibility, and rapid renal clearance, endowing it with a great potential for future translational research.

Photodynamic therapy (PDT) can ablate the targeted diseased cells or tissue using photosensitizer (PS) generated reactive oxygen species (ROS) once PS is excited by the light with specific wavelength,[1] while the PS remains benign in the absence of light excitation. As compared with traditional cancer treatments such as chemotherapy and radiotherapy, PDT is featured with remarkable advantages, including minimal invasiveness, low side effects, etc. Therefore, PDT is recognized as a promising treatment strategy.[2,3] In recent years, various PSs have been designed and synthesized for cancer therapy,[4,5] e.g., organic semiconducting nanoparticles (NPs) based PDT could achieve good anticancer performance.[6–8] Porphyrin and its derivatives are still the most widely used PSs,[9,10] particularly in the clinical oncology treatment including breast cancer, lung cancer, etc.[1–3] However, the

W. Pang, P. Jiang, S. Ding, Prof. B. Gu, Prof. X. Wei
School of Biomedical Engineering and State Key Laboratory of Oncogenes and Related Genes
Shanghai Jiao Tong University
1954 Huashan Road, Shanghai 200030, China
E-mail: bobogu@sjtu.edu.cn; xwei01@sjtu.edu.cn

Dr. Z. Bao
Department of Obstetrics and Gynecology, Ren Ji Hospital
School of Medicine
Shanghai Jiao Tong University
Shanghai 200127, China

Dr. Z. Bao
Shanghai Key Laboratory of Gynecologic Oncology, Ren Ji Hospital
School of Medicine
Shanghai Jiao Tong University
Shanghai 200127, China

N. Wang
Department of 2nd Dental Center
Shanghai Ninth People's Hospital
College of Stomatology
Shanghai Jiao Tong University
School of Medicine
Shanghai 200011, China

Prof. H. Wang
Department of Oncology
Shanghai General Hospital
Shanghai Jiao Tong University School of Medicine
Shanghai 200080 China

Prof. J. Qu
Key Laboratory of Optoelectronic Devices and Systems of Ministry of Education and Guangdong Province
College of Physics and Optoelectronic Engineering
Shenzhen University
Shenzhen 518060, China

Prof. D. Wang
State Key Laboratory of Organic-Inorganic Composites
Beijing University of Chemical Technology
Beijing 100029, China
E-mail: wangdan@mail.buct.edu.cn

Prof. X. Wei
Beijing Advanced Innovation Center for Biomedical Engineering
Beihang University
Beijing 100083, China

The ORCID identification number(s) for the author(s) of this article can be found under https://doi.org/10.1002/adhm.202000607

DOI: 10.1002/adhm.202000607

treatment efficiency of PDT using porphyrin and porphyrin-based PSs is limited since these PSs possess hydrophobic and rigid planar structures and consequently suffer from aggregation-caused quenching (ACQ) issue in aqueous media.[11] Fluorogens with aggregation-induced emission characteristics (AIEgens) can emit bright fluorescence in the aggregated state,[11,12] making AIEgens excellent candidates to overcome ACQ issue. By tuning the singlet-triplet energy gap, AIEgens could generate ROS efficiently for PDT applications.[13–17] Another solution to overcome ACQ issue is utilization of inorganic nanomaterials,[4] including graphene quantum dots (QDs),[18] black phosphorus,[19] metal–organic framework nanodots,[20] semiconducting nanoparticles (NPs),[21] etc., which could serve as PSs directly, and the ROS quantum yield of graphene QDs even could reach ≈1.3,[18] which is much higher than that of their organic counterparts.

It is well known that the intracellular location of PSs can affect the final PDT performance.[22] Various organelles-targeted PSs, including mitochondria,[23] lysosomes,[24] endoplasmic reticulum,[25] etc., have been synthesized and studied. Recently, the nucleus-targeted PSs were designed and synthesized to further improve PDT,[26–28] e.g., the obtained photocytotoxicity of Chlorin e6 (Ce6), which is conjugated with nuclear localization signals to facilitate the nucleus penetration, could even be enhanced over 2000-fold.[28] The latest advances show that nucleolus plays an important role in resisting cell death, activating invasion and metastasis of cancer cells, making nucleolus a more efficient and ideal site for cancer treatment,[29] e.g., the nucleolus-targeted chemotherapy using UNBS1450 (currently in Phase I clinical trials) could obtain ≈100-fold enhanced treatment effects as compared with DNA-interacted chemotherapy by oxaliplatin, irinotecan, and etoposide.[30,31] Thus, it can be deduced that nucleolus-targeted PDT should achieve enhanced therapeutic effects for cancer as compared with other organelles targeted PDT. Despite the significant role of nucleolus in cancer therapy, nucleolus-targeted PSs are still very rare. PSs were conjugated with some inorganic NPs with intrinsic nucleolus-targeting feature, e.g. nucleolus-targeted CD-PpIX (CD: carbon dots, PpIX: protoporphyrin IX) nanocomposite achieved remarkably enhanced PDT treatment as compared with free PpIX located in cytosol.[32] However, the size of formed PDT agents is much larger than 5 nm, making it difficult to be rapidly cleared.[33,34] Moreover, conjugation process is complicated and time consuming and also would significantly lower the nucleolus-targeting capability and subsequently PDT efficiency. Thus, it is meaningful and urgent to design and synthesize novel PDT agents with high nucleolus-targeting capability and rapid clearance to achieve enhanced treatment performance and biosafety.

Herein, we report newly engineered carbon dots (C-dots) photosensitizer with intrinsic ROS generation and nucleolus-targeting capability. The C-dots show high ROS generation efficiency and fluorescence quantum yield, outstanding in vitro and in vivo anticancer performance at a low dose of C-dots and light irradiation due to the nucleolus-targeting induced photocytotoxicity enhancement. Meanwhile, the excellent biocompatibility and rapid renal clearance of C-dots guarantee their potential for clinical anticancer therapy applications.

The C-dots have been designed and synthesized as either bioimaging or PDT agents.[35–37] Here, we proposed and demonstrated, for the first time, the C-dots with both nucleolus-targeting and ROS generation capability for nucleolus-targeted photodynamic anticancer therapy. As shown in **Figure 1**A, the C-dots could penetrate nucleolus and generate ROS within nucleolus under light irradiation, enabling enhanced image-guided photodynamic anticancer therapy. The C-dots were prepared via reaction of citric acid (CA) and ethylenediamine (EDA) by refluxing the reaction mixture.[38] In the typical procedure, the amounts of reactants were 2 g of CA and 3 mL of EDA. The mole mass ratio of CA/EDA was ≈1:4.5. Then the condensation was carried out with an excess of EDA, which was removed by volatilization during the reaction process. Then pure C-dots were obtained once the product was air-cooled down to room temperature, without any further purification. The synthesized C-dots were studied by dynamic light scattering measurement and transmission electron microscope (Figure S1, Supporting Information). The measured average size of 2 nm enables rapid renal clearance of C-dots. The synthesized C-dots show a broad absorption range (350–700 nm) with a main absorption peak at 350 nm and a shoulder peak at 450 nm as shown in Figure 1B. The C-dots have excitation-dependent emission as show in Figure 1C. The quantum yield of the synthesized C-dots measured at 350 nm was 42.7%, such high quantum yield enables image-guided PDT during treatment. The photostability of C-dots was also studied by measuring the absorption spectra (Figure S2, Supporting Information). After 30 min continuous irradiation (400–700 nm, 100 mW cm^{-2}), the absorption of C-dots was decreased slightly. Thus, it can be deduced that C-dots have good photostability for biomedical applications.

The ROS generation efficiency of C-dots (25 μg mL^{-1}) in aqueous media was subsequently investigated under the light irradiation (400–700 nm, 70 mW cm^{-2}) using 9,10-anthracenediyl-bis(methylene)dimalonic acid (ABDA) (50×10^{-6} M) as the ROS indicator. As shown in Figure 1D, ABDA was almost decomposed after 10 min illumination, indicating the ROS generation capability of C-dots. In order to quantitatively study the ROS quantum yield (Φ) of C-dots, a commercial PS, i.e., Ce6 ($\Phi_{Ce6} = 0.66$ in aqueous media[39]) was selected as the reference for measurement. The obtained ROS quantum yield of C-dots is 0.048 (Figure S3, Supporting Information), which is lower than organic semiconducting materials,[40] but much higher than that of one US Food and Drug Administration (FDA) approved approved PS, i.e., indocyanine green (ICG, $\Phi_{ICG} = 0.002$).[41]

To explore the intracellular localization, C-dots (200 μg mL^{-1}) were incubated with 4T1 cells for different time. As shown in **Figure 2**A, after 30 min incubation, the fluorescent signals of C-dots were observed in some round areas, i.e., nucleoli, but no any lysosomal/endosomal entrapment could be observed, indicating that the C-dots penetrated the nucleolus via a direct and fast movement.[42] Meanwhile, with increment of incubation time, the fluorescence intensity of C-dots located in nucleolus was further enhanced, improving the signal-to-noise ratio. Furthermore, the C-dots were still located at nucleoli even after staining for 5 h. These results suggest that the C-dots inherently possess the nucleolus-targeting capability. To assess the nucleolus-targeting universality, C-dots were also incubated with other cancerous cells including HeLa and H520. As shown in

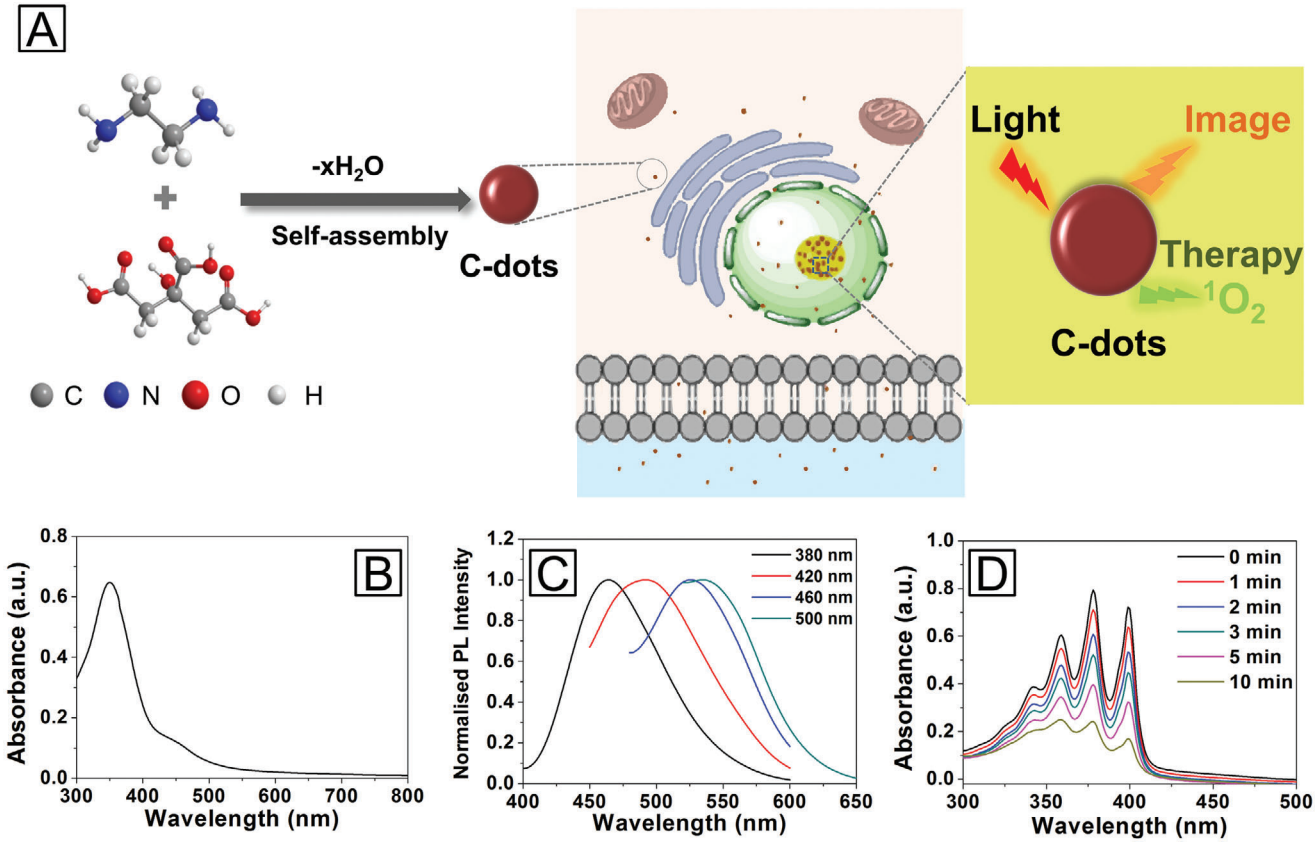

Figure 1. A) Schematics of synthetic procedure of C-dots and corresponding nucleolus-targeted photodynamic anticancer therapy. B) The UV–vis absorption spectrum of C-dots. C) The fluorescence emission spectra of C-dots under different excitation wavelengths. D) UV–vis spectra of ABDA and C-dots under light irradiation for different time (400–700 nm, ≈70 mW cm^{-2}). [ABDA] = 50 × 10^{-6} M, [C-dots] = 25 μg mL^{-1}.

Figure S4 in the Supporting Information, all nucleoli in these treated cells were specifically stained by C-dots (200 μg mL^{-1}) with green fluorescence, which was also enhanced with increment of incubation time, demonstrating that the C-dots possess highly universal and specific nucleolus-targeting capability. To identify the localization of C-dots, the SYTO RNASelect (one commercial probe for nucleolus imaging) was selected to costain 4T1 cells with C-dots. As shown in Figure 2B, the fluorescence of C-dots was totally overlapped with that of the SYTO RNASelect. It means that the C-dots could specifically stain the nucleolus, indicating the nucleolus-targeting capability of C-dots. The colocalization experiment was performed in HeLa cells as shown in Figure S5 in the Supporting Information, the results also showed the nucleolus-targeting capability of C-dots. It is well known that most RNAs and some DNAs accumulate in the nucleolus. In order to further study the nucleolus-targeting capability of C-dots, the cellular imaging performances of C-dots and one commercially available nucleus-targeting dyes, i.e., Hoechst 33342 were compared. As shown in Figure 2C, Hoechst 33342 could stain the whole nucleus and part of nucleoli in unfixed 4T1 cells (living cells) and the whole nucleus except nucleoli in fixed 4T1 cells, while C-dots could light-up only nucleoli specifically, which could be confirmed with bright field and merged images, in both unfixed and fixed cells. Similar results were also observed in HeLa cells as shown in Figure S6 in the Supporting Information, Hoechst 33342 could stain the whole nucleus in unfixed and fixed 4T1 cells, while C-dots could specifically light-up the nucleoli in both unfixed and fixed cells. These results indicate the highly specific nucleolus-targeting capability of C-dots.

In order to study the nucleolus-targeting mechanism of C-dots, ribonuclease RNase and DNase were selected to hydrolyze RNA and DNA of 4T1 cells respectively, followed by the targeting capability comparison of C-dots and Hoechst 33342. As shown in Figure 2C, when the cells were digested by DNase, the whole nucleoli and part of nucleoli were still stained by C-dots and Hoechst 33342, respectively. Once the cells were digested by RNase, both C-dots and Hoechst 33342 would stain the whole nucleus. The nucleus and nucleolus region could be confirmed from the bright field images. The digest experiments were also performed on HeLa cells as shown in Figure S6 in the Supporting Information. Once HeLa cells were digested by RNase, C-dots and Hoechst 33342 would also stain the whole nucleus. It can be deduced that C-dots could selectively target RNA instead of DNA.

2',7'-Dchlorofluorescin-diacetate (DCFH-DA) was selected as the ROS indicator to study the intracellular ROS generation capability of C-dots. After incubating either with both C-dots and DCFH-DA, or with DCFH-DA alone, the 4T1 cells were irradiated and imaged with confocal laser scanning microscopy. As shown in Figure 2D and Figure S7 in the Supporting Information, strong fluorescent signal of dichlorofluorescein (DCF) was

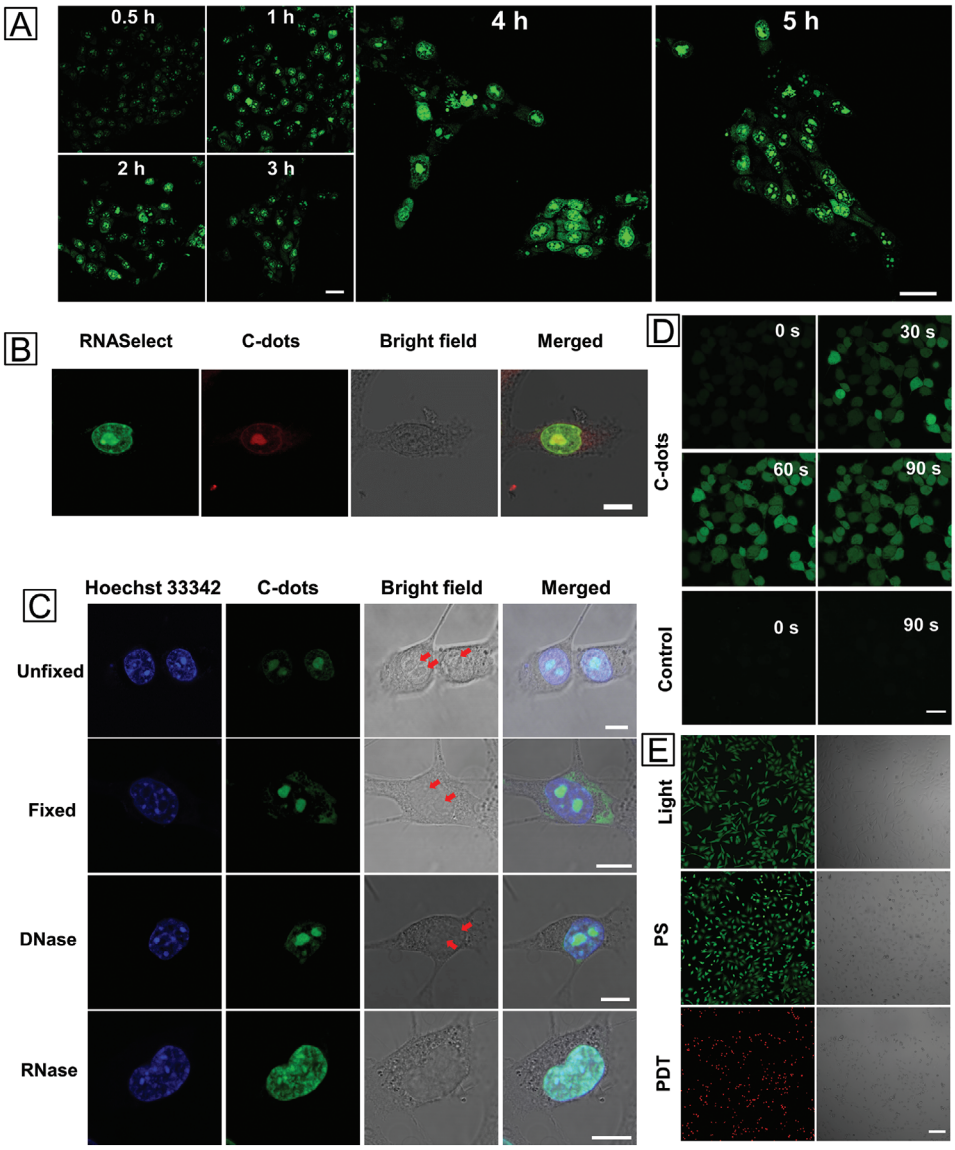

Figure 2. A) Time-sequenced fluorescence images of C-dots (0.2 mg mL^{-1}) stained 4T1 cells (0.5, 1, 2, 3, 4, 5 h). Ex: 488 nm, Em: 500–550 nm. Scale bar: 50 μm. B) Fluorescence images of 4T1 cells stained with both RNASelect and C-dots, and bright field and merged images. RNASelect channel (Ex: 488 nm, Em: 510–540 nm), C-dots channel (Ex: 552 nm, Em: 560–590 nm). [RNASelect] = 10×10^{-6} M, [C-dots] = 200 μg mL^{-1}. Scale bar: 10 μm. C) Fluorescence images of unfixed, fixed, DNase digested, and RNase digested 4T1 cells treated with C-dots and Hoechst 33342, and bright field and merged images. Hoechst 33342 channel (Ex: 405 nm, Em: 415–485 nm), C-dots channel (Ex: 488 nm, Em: 500–610 nm). [C-dots] = 200 μg mL^{-1}, [Hoechst 33342] = 5 μg mL^{-1}, [DNase] = 25 μg mL^{-1}, [RNase] = 25 μg mL^{-1}. Scale bar: 10 μm, red arrows indicate nucleolus. D) Study of the intracellular ROS generation capability of C-dots (200 μg mL^{-1}) under light irradiation (488 nm laser, ≈0.1 mW). DCF (Ex: 488 nm; Em: 500–550 nm). [DCFH-DA] = 5×10^{-6} M. Scale bar: 50 μm. E) Viability of HeLa cells treated with/without C-dots followed by light irradiation for 30 min (400–700 nm; 150 mW cm^{-2}) or only treated with C-dots. Calcein-AM (Ex: 488 nm; Em: 505–525 nm) and propidium iodide (PI) (Ex: 552 nm; Em: 605–625 nm), [C-dots] = 500 μg mL^{-1}, [Calcein-AM] = 2×10^{-6} M, [PI] = 2×10^{-6} M. Scale bar: 200 μm.

observed from the cells incubated with both C-dots and DCFH-DA. Since DCF could permeate nucleus, the whole cell would be stained once ROS oxidized DCFH-DA to DCF. In the initial scans, the fluorescent intensity of DCF increased quickly and reached a plateau when the scan times reached 60 s and then even suffered from slight photobleaching when further irradiation was performed, demonstrating effective and rapid intracellular ROS generation of C-dots. In contrast, there was no any fluorescent signal in the absence of C-dots, eliminating the possibility of any laser induced interference to the obtained results.

Before conducting in vitro and in vivo photodynamic anticancer therapy, the biocompatibility of C-dots was evaluated. 4T1 cells were incubated with C-dots of various concentrations for different incubation time, and then standard MTT (3-(4,5-Dimethylthiazol-2-yl)-2,5-diphenyltetrazolium bromide) assay was used to assess the cell viability. As shown in Figure S8 in the Supporting Information, there was no significant

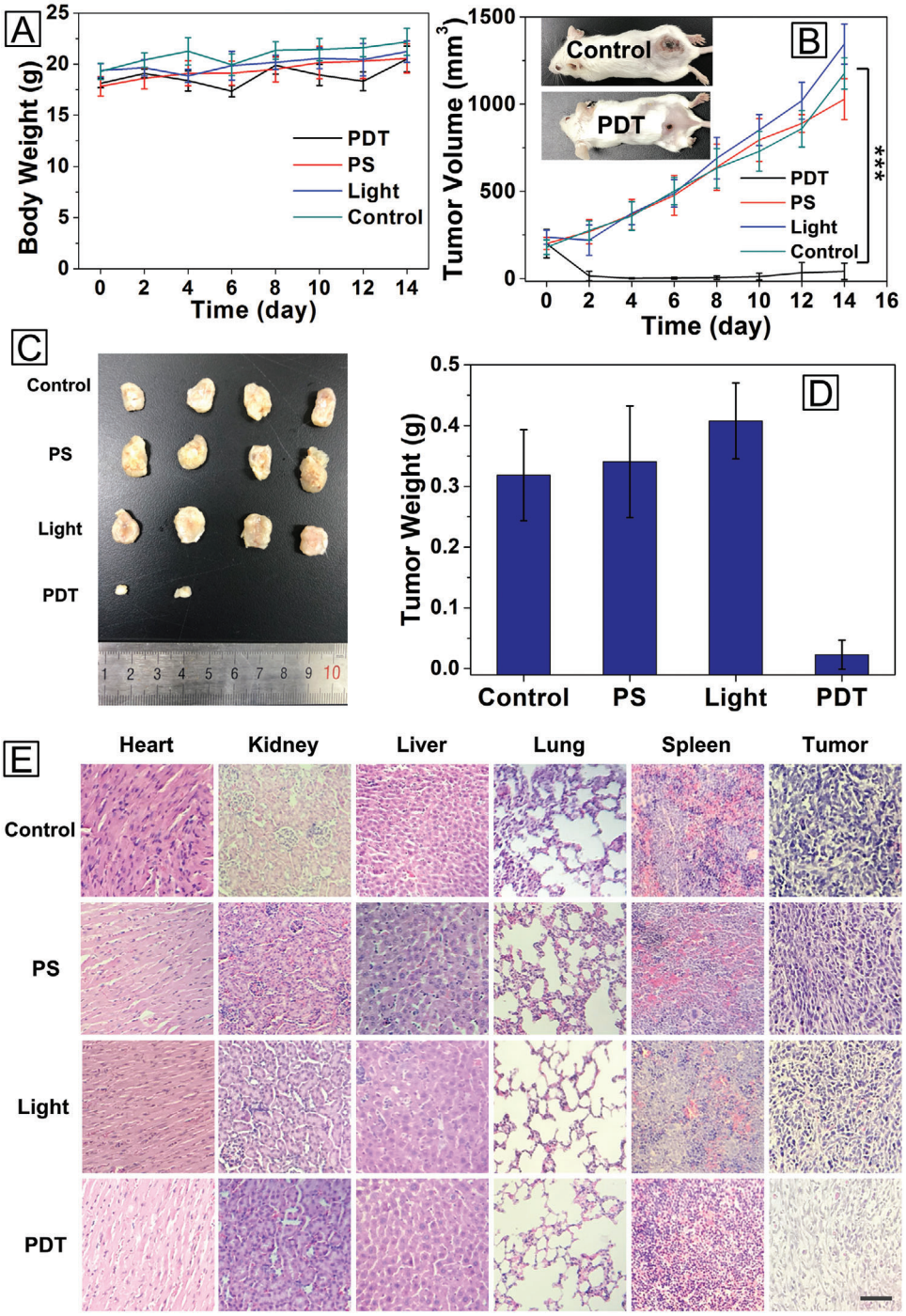

Figure 3. A) Body weight for different groups of mice ($n = 4$). B) Tumor volume for different groups of mice. Error bar indicates SEM (SEM: standard error of mean, ***, $P < 0.001$, $n = 4$). The insets show the representative photographs of mice from PDT and Control groups on day 14 post-treatment, respectively. C) The image of excised tumors on day 14 post-treatment. D) Quantitative analysis of tumor weight on day 14 post-treatment ($n = 4$). E) Histologic studies on tumor and major organs of mice from different groups. Scale bar: 50 μm.

difference between the control cells and the cells treated with C-dots in the concentration range of 50–300 μg mL^{-1} for 24 and 48 h, indicating excellent biocompatibility.

To analyze the in vitro cancer cells ablation efficiency of C-dots, HeLa cells were incubated with/without C-dots (500 μg mL^{-1}) for 24 h. After light irradiation (400–700 nm, 150 mW cm^{-2}, 30 min), the cells were stained with calcein-acetoxymethyl ester (calcein-AM) and propidium iodide (PI) for viability analysis using confocal laser scanning microscopy. As shown in Figure 2E, all cells treated with both C-dots and light irradiation, i.e., PDT

group were PI-positive, since PI is a fluorescent nucleic acid stain that can permeate only the damaged membranes, it can be deduced that membranes of nucleus were damaged by PDT effect, demonstrating the good anticancer activity. Meanwhile, the cells treated with only C-dots or light irradiation, i.e., PS group and Light group showed the calcein-AM fluorescence, indicating that C-dots or light irradiation alone did not induce any cellular phototoxicity.

The synthesized C-dots have shown good nucleolus-targeting capability, high intracellular ROS generation efficiency and biocompatibility, and efficient in vitro PDT effect, making C-dots a promising in vivo PDT agent. The tumor-bearing mouse model was established by subcutaneously inoculating 4T1 breast cancer cells. In PDT group, mice were intratumorally injected with C-dots (10 mg kg^{-1}) and immediately irradiated with light (400–700 nm; 100 mW cm^{-2}; 20 min). While the control groups were composed of mice without any treatment (Control group), mice administered with C-dots but not light irradiation (PS group) and mice subjected to light irradiation (Light group). Moreover, the temperature during treatment was monitored by an IR thermal camera. As shown in Figure S9 in the Supporting Information, with increment of treatment time, the temperature at tumor site rose slowly. After 20 min irradiation, the temperature reached 40.7 °C, which was lower than the temperature required for photothermal therapy (PTT).[43] Thus, PTT induced interference could be efficiently eliminated from this treatment. After treatment, the mice weight and tumor size were measured every 2 d. There was no any significant body weight loss for all groups within 2 weeks as shown in **Figure 3**A. It was observed that the tumor size of PDT treated mice was obviously decreased, while that of other groups (including Control, PS and Light groups) kept increasing quickly as shown in Figure 3B and Figure S10 in the Supporting Information. All mice were sacrificed on day 14, the practical morphology and tumor weight were shown in Figure 3C,D. The tumors of PDT group were significantly reduced, even completely disappeared, confirming the effectiveness of C-dots based PDT. Previously, PDT could only suppress tumor growth instead of reducing the tumor size. The significantly reduced tumor size by nucleolus-targeted PDT using C-dots proved their improvement in cancer treatment. To observe histological changes, tumors were also harvested for hematoxylin and eosin staining. As shown in Figure 3E and Figure S11 in the Supporting Information, there were no any significant changes in the Control, PS and Light groups, and the nucleus and nucleolus were almost intact. In PDT group, dissociation of nucleus and nucleus and formation of apoptotic bodies were observed, which was consistent with previous studies.[44] Moreover, major organs including heart, kidneys, liver, lung, and spleen were also collected for analysis. There were no any signs of organ lesions in mice of all groups. These results indicate that C-dots have no obvious in vivo toxicity.

In addition, pharmacokinetics is another key factor to evaluate PSs. As shown in **Figure 4**A, 10 min after intratumorally injection of C-dots (10 mg kg^{-1}), strong fluorescent signals were

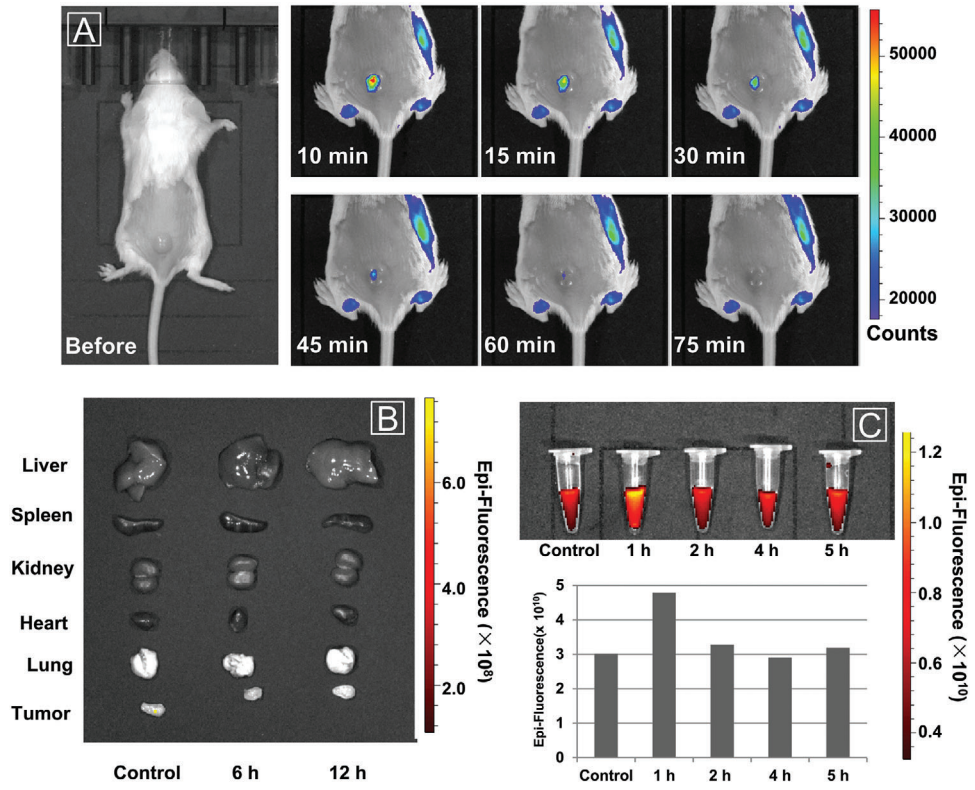

Figure 4. A) Time-dependent in vivo fluorescence images of tumor-bearing mice before and after intratumorally injection of C-dots (10 mg kg^{-1}). B) Ex vivo fluorescence image of major organs and tumors from mice at 6 and 12 h post intravenously injection of C-dots (4 mg mL^{-1}, 50 µL, 10 mg kg^{-1}). C) The fluorescence image and quantitative fluorescence analysis of urine samples postinjection of C-dots (10 mg kg^{-1}). Ex: 488 nm, Em: 500–550 nm.

captured at the tumor site and then the fluorescence intensity decreased quickly. There was even no fluorescent signal 1 h after injection. In order to study the in vivo biodistribution of C-dots, the ex vivo fluorescence images of major organs and tumors excised from control and treated mice at 6 and 12 h post intravenously injection of C-dots (4 mg mL^{-1}, 50 µL, 10 mg kg^{-1}) were captured. As shown in Figure 4B, neither major organs nor tumor tissue showed any fluorescent signal of C-dots. The same results were also achieved when the C-dots were intratumorally injected as shown in Figure S12 in the Supporting Information. It means that C-dots could be cleared out of the body. Considering the ultrasmall size (2 nm), C-dots could be cleared out via the renal route into urine. Then the urine of the C-dots treated mice was collected every one hour after injections and then imaged. As shown in Figure 4D, only the urine collected in the first 1 h showed strong fluorescent signal of C-dots, while the fluorescence intensity of other urine samples is almost same as that of control samples. These results indicated that C-dots were cleared out via the renal route into urine with high clearance rate, which is comparable with that of cyclodexrin molecules and much better than that of gold nanoclusters and Cornel dots.[45] Excellent in vivo biocompatibility and rapid renal clearance endow C-dots with good biosafety and potential for clinical applications.

In summary, we designed and synthesized novel C-dots with both intrinsic nucleolus-targeting and ROS generation capability for the first time. Considering that the C-dots generated ROS is located within nucleolus and nucleolus is a more efficient tumor treatment site, an enhanced in vitro and in vivo photodynamic anticancer therapy performance was achieved at a low dose of C-dots and light irradiation. Moreover, the developed C-dots photosensitizer possesses unique advantages including high ROS generation efficiency and fluorescence quantum yield, excellent in vitro and in vivo biocompatibility, rapid renal clearance, making C-dots promising in practical PDT applications. This study highlights the great potential of C-dots photosensitizers for future translational research.

Supporting Information

Supporting Information is available from the Wiley Online Library or from the author.

Acknowledgements

W.P. and P.J. contributed equally to this work. This work was supported by the Natural Science Foundation of China (61805135, 61425006, 81772802, 61835009, and 21808009), Pujiang Talents Program (18PJ1405100), Shanghai Jiao Tong University (ZH2018QNA43, YG2017MS19, and YG2016MS22), and Program of Shanghai Technology Research Leader (17XD1402200). All the animal care and experimental procedures were approved by the Ethical Committee of Animal Experiments in the School of Biomedical Engineering, Shanghai Jiao Tong University.

Conflict of Interest

The authors declare no conflict of interest.

Keywords

cancer therapy, carbon dots, nucleolus targeting, photodynamic therapy, renal clearance

Received: April 13, 2020
Revised: May 17, 2020
Published online: June 16, 2020

[1] D. E. J. G. J. Dolmans, D. Fukumura, R. K. Jain, *Nat. Rev. Cancer* **2003**, *3*, 380.
[2] P. Agostinis, K. Berg, K. A. Cengel, T. H. Foster, A. W. Girotti, S. O. Gollnick, S. M. Hahn, M. R. Hamblin, A. Juzeniene, D. Kessel, M. Korbelik, J. Moan, P. Mroz, D. Nowis, J. Piette, B. C. Wilson, J. Golab, *Ca-Cancer J. Clin.* **2011**, *61*, 250.
[3] S. B. Brown, E. A. Brown, I. Walker, *Lancet Oncol.* **2004**, *5*, 497.
[4] S. S. Lucky, K. C. Soo, Y. Zhang, *Chem. Rev.* **2015**, *115*, 1990.
[5] M. R. Detty, S. L. Gibson, S. J. Wagner, *J. Med. Chem.* **2004**, *47*, 3897.
[6] J. C. Li, D. Cui, J. G. Huang, S. S. He, Z. B. Yang, Y. Zhang, Y. Luo, K. Y. Pu, *Angew. Chem., Int. Ed.* **2019**, *58*, 12680.
[7] Y. Y. Jiang, J. C. Li, Z. L. Zeng, C. Xie, Y. Lyu, K. Y. Pu, *Angew. Chem., Int. Ed.* **2019**, *58*, 8161.
[8] J. Li, D. Cui, Y. Jiang, J. Huang, P. Cheng, K. Pu, *Adv. Mater.* **2019**, *31*, 1905091.
[9] M. Ethirajan, Y. H. Chen, P. Joshi, R. K. Pandey, *Chem. Soc. Rev.* **2011**, *40*, 340.
[10] B. Gu, A. Pliss, A. N. Kuzmin, A. Baev, T. Y. Ohulchanskyy, J. A. Damasco, K. T. Yong, S. C. Wen, P. N. Prasad, *Biomaterials* **2016**, *104*, 78.
[11] J. Mei, N. L. C. Leung, R. T. K. Kwok, J. W. Y. Lam, B. Z. Tang, *Chem. Rev.* **2015**, *115*, 11718.
[12] J. Mei, Y. N. Hong, J. W. Y. Lam, A. J. Qin, Y. H. Tang, B. Z. Tang, *Adv. Mater.* **2014**, *26*, 5429.
[13] S. D. Xu, Y. Y. Yuan, X. L. Cai, C. J. Zhang, F. Hu, J. Liang, G. X. Zhang, D. Q. Zhang, B. Liu, *Chem. Sci.* **2015**, *6*, 5824.
[14] B. Gu, W. B. Wu, G. X. Xu, G. X. Feng, F. Yin, P. H. J. Chong, J. L. Qu, K. T. Yong, B. Liu, *Adv. Mater.* **2017**, *29*, 1701076.
[15] B. Gu, K. T. Yong, B. Liu, *Small Methods* **2018**, *2*, 1700392.
[16] W. B. Wu, D. Mao, F. Hu, S. D. Xu, C. Chen, C. J. Zhang, X. M. Cheng, Y. Y. Yuan, D. Ding, D. L. Kong, B. Liu, *Adv. Mater.* **2017**, *29*, 1700548.
[17] F. Hu, S. D. Xu, B. Liu, *Adv. Mater.* **2018**, *30*, 1801350.
[18] J. C. Ge, M. H. Lan, B. J. Zhou, W. M. Liu, L. Guo, H. Wang, Q. Y. Jia, G. L. Niu, X. Huang, H. Y. Zhou, X. M. Meng, P. F. Wang, C. S. Lee, W. J. Zhang, X. D. Han, *Nat. Commun.* **2014**, *5*, 4596.
[19] H. Wang, X. Z. Yang, W. Shao, S. C. Chen, J. F. Xie, X. D. Zhang, J. Wang, Y. Xie, *J. Am. Chem. Soc.* **2015**, *137*, 11376.
[20] H. Wang, D. Q. Yu, J. Fang, C. C. Cao, Z. Liu, J. S. Ren, X. G. Qu, *ACS Nano* **2019**, *13*, 9206.
[21] H. J. Zhu, J. C. Li, X. Y. Qi, P. Chen, K. Y. Pu, *Nano Lett.* **2018**, *18*, 586.
[22] A. P. Castano, T. N. Demidova, M. R. Hamblin, *Photodiagn. Photodyn. Ther.* **2004**, *1*, 279.
[23] W. Lv, Z. Zhang, K. Y. Zhang, H. R. Yang, S. J. Liu, A. Q. Xu, S. Guo, Q. Zhao, W. Huang, *Angew. Chem., Int. Ed.* **2016**, *55*, 9947.
[24] H. Y. Huang, B. L. Yu, P. Y. Zhang, J. J. Huang, Y. Chen, G. Gasser, L. N. Ji, H. Chao, *Angew. Chem., Int. Ed.* **2015**, *54*, 14049.
[25] J. S. Nam, M. G. Kang, J. Kang, S. Y. Park, S. J. C. Lee, H. T. Kim, J. K. Seo, O. H. Kwon, M. H. Lim, H. W. Rhee, T. H. Kwon, *J. Am. Chem. Soc.* **2016**, *138*, 10968.
[26] L. M. Pan, J. A. Liu, J. L. Shi, *Adv. Funct. Mater.* **2014**, *24*, 7318.
[27] R. Vankayala, C. L. Kuo, K. Nuthalapati, C. S. Chiang, K. C. Hwang, *Adv. Funct. Mater.* **2015**, *25*, 5934.
[28] T. V. Akhlynina, D. A. Jans, A. A. Rosenkranz, N. V. Statsyuk, I. Y. Balashova, G. Toth, I. Pavo, A. B. Rubin, A. S. Sobolev, *J. Biol. Chem.* **1997**, *272*, 20328.
[29] N. Hein, K. M. Hannan, A. J. George, E. Sanij, R. D. Hannan, *Trends Mol. Med.* **2013**, *19*, 643.
[30] T. Mijatovic, N. De Neve, P. Gailly, V. Mathieu, B. Haibe-Kains, G. Bontempi, J. Lapeira, C. Decaestecker, V. Facchini, R. Kiss, *Mol. Cancer Ther.* **2008**, *7*, 1285.

[31] S. J. Woods, K. M. Hannan, R. B. Pearson, R. D. Hannan, *Biochim. Biophys. Acta, Gene Regul. Mech.* **2015**, *1849*, 821.
[32] X. W. Hua, Y. W. Bao, F. G. Wu, *ACS Appl. Mater. Interfaces* **2018**, *10*, 10664.
[33] B. Wang, X. He, Z. Y. Zhang, Y. L. Zhao, W. Y. Feng, *Acc. Chem. Res.* **2013**, *46*, 761.
[34] X. L. Huang, F. Zhang, L. Zhu, K. Y. Choi, N. Guo, J. X. Guo, K. Tackett, P. Anilkumar, G. Liu, Q. M. Quan, H. S. Choi, G. Niu, Y. P. Sun, S. Lee, X. Y. Chen, *ACS Nano* **2013**, *7*, 5684.
[35] N. Panwar, A. M. Soehartono, K. K. Chan, S. W. Zeng, G. X. Xu, J. L. Qu, P. Coquet, K. T. Yong, X. Y. Chen, *Chem. Rev.* **2019**, *119*, 9559.
[36] S. N. Fan, X. T. Zheng, Q. Zhan, H. H. Zhang, H. L. Shao, J. X. Wang, C. B. Cao, M. F. Zhu, D. Wang, Y. P. Zhang, *Nano-Micro Lett.* **2019**, *11*, 75.
[37] J. C. Ge, Q. Y. Jia, W. M. Liu, M. H. Lan, B. J. Zhou, L. Guo, H. Y. Zhou, H. Y. Zhang, Y. Wang, Y. Gu, X. M. Meng, P. F. Wang, *Adv. Healthcare Mater.* **2016**, *5*, 665.
[38] D. Wang, Z. Y. Wang, Q. Q. Zhan, Y. Pu, J. X. Wang, N. R. Foster, L. M. Dai, *Engineering* **2017**, *3*, 402.
[39] R. W. Redmond, J. N. Gamlin, *Photochem. Photobiol.* **1999**, *70*, 391.
[40] J. C. Li, K. Y. Pu, *Chem. Soc. Rev.* **2019**, *48*, 38.
[41] H. Gao, R. Liu, F. P. Gao, Y. L. Wang, X. L. Jiang, X. Y. Gao, *ACS Nano* **2014**, *8*, 7260.
[42] H. Nakamura, S. Watano, *KONA Powder Part. J.* **2018**, *35*, 49.
[43] D. Jaque, L. M. Maestro, B. del Rosal, P. Haro-Gonzalez, A. Benayas, J. L. Plaza, E. M. Rodriguez, J. G. Sole, *Nanoscale* **2014**, *6*, 9494.
[44] K. Smetana, H. Cajthamlova, D. Grebenova, Z. Hrkal, *J. Photochem. Photobiol., B* **2000**, *59*, 80.
[45] J. G. Huang, J. C. Li, Y. Lyu, Q. Q. Miao, K. Pu, *Nat. Mater.* **2019**, *18*, 1133.